*Int. J. Heat Mass Transfer.* Vol. 32, No. 9, pp. 1719–1731, 1989
Printed in Great Britain

0017–9310/89 $3.00+0.00


# The modelling of heat, mass and solute transport in solidification systems

V. R. VOLLER and A. D. BRENT
Department of Civil and Mineral Engineering, Mineral Resources Research Center, University of Minnesota, Minneapolis, MN 55455, U.S.A.

and

C. PRAKASH
Corporate Research and Development Center, General Electric, Schenectady, NY 12301, U.S.A.

(*Received* 4 *August* 1988 *and in final form* 13 *February* 1989)

**Abstract**—The aim of this paper is to explore the range of possible one-phase models of binary alloy solidification. Starting from a general two-phase description, based on the two-fluid model, three limiting cases are identified which result in one-phase models of binary systems. Each of these models can be readily implemented in standard single phase flow numerical codes. Differences between predictions from these models are examined. In particular, the effects of the models on the predicted macro-segregation patterns are evaluated.

## 1. INTRODUCTION

### 1.1. *An example solidification system*

SINCE the pioneering work of Eyres *et al.* [1], the modelling of solidification systems has been a major area of research in the heat and mass transfer community. A comprehensive example of a solidification system is one based on a binary system (e.g. a binary alloy). Consider such a system in the liquid state contained in a rectangular cavity insulated on three sides depicted in Fig. 1. At time $t = 0$ the left face is lowered to a temperature $T_{cold} < T_L$ (the liquidus temperature). At later times three regions will exist in the cavity (see Fig. 1); a full solid region, a solid+liquid mushy region, and a full liquid region. In metals the mushy region usually has a dendritic crystalline structure. The mushy region is bounded by liquidus and solidus (or eutectic) isotherms. As solidification proceeds, the solute phase is rejected from the solidifying dendrites in the mushy region. On the local scale this solute is redistributed by diffusion transport. Such a redistribution of solute is referred to as micro-segregation. Thermo-solutal convection currents, however, are also present in the mushy region. This flow carries the expelled solute away from the site of rejection and results in so-called macro-segregation. From a practical viewpoint, the nature and extent of the macro-segregation will determine the quality of the final product. Macro-segregation is an important research area and extensive studies have been conducted to elucidate the controlling mechanisms [2–7].

### 1.2. *Modelling of solidification systems*

Many of the earlier models of solidification systems were one-dimensional and only considered heat conduction (see the reviews in refs. [8, 9]). In two- or three-dimensional solidification systems, however, fluid flow effects also need to be considered. This requires the coupled solution of the Navier–Stokes and energy equations. An early numerical approach for dealing with convection–diffusion controlled isothermal phase changes is reported by Sparrow *et al.* [10]. Subsequent attempts, for this class of problem, fall into two broad categories; those that employ a temperature formulation along with a deforming–transformed mesh [11–13], and those that employ an enthalpy formulation on a fixed computational mesh [14–16].

Isothermal phase change problems occur only in pure metal systems. However, as noted above, binary alloy systems are characterized by the presence of a mushy region. Models for such mushy systems have been presented in refs. [17, 18].

The mushy models proposed in refs. [17, 18] treat the mushy region relationship between the liquid mass fraction ($f_l$) and temperature ($T$) in an arbitrary manner. In a binary system, however, the $f_l$–$T$ relationship is a function of the local solute concentration. Due to the fact that the solute is redistributed as solidification occurs (i.e. macro-segregation), a comprehensive model of a solidification system requires the solution of a solute transport equation along with the Navier–Stokes and energy equations. Such models have only recently been proposed [19–25].

### 1.3. *Aims of the present work*

The binary solidification system used as an example in this work is essentially a solid–liquid two-phase system. In order for this system to be fully described,

## NOMENCLATURE

| | |
|---|---|
| $c$ | specific heat |
| $C$ | concentration of solute (mass fraction) |
| $C_e$ | eutectic concentration of solute |
| $C_{mix}$ | mixture concentration |
| $\mathbf{F}$ | external body force ensuring satisfaction of two-phase momentum equations |
| $g$ | volume fraction |
| $g_r$ | gravity |
| $h$ | sensible enthalpy |
| $H$ | phase enthalpy |
| $\Delta H$ | difference in phase enthalpies |
| $K$ | thermal conductivity |
| $K_0$ | permeability coefficient in Carman–Kozeny equations |
| $L$ | latent heat of fusion |
| $P$ | pressure |
| $S$ | source term in conservation equations |
| $t$ | time |
| $T$ | temperature |
| $T_e$ | eutectic temperature |
| $T_L$ | liquidus temperature |
| $T_M$ | melting point of pure solute |
| $T_s$ | solidus temperature |
| $\mathbf{u}$ | velocity vector |
| $u$ | $x$-direction velocity |
| $v$ | $y$-direction velocity |
| $V$ | volume of phase |
| $w$ | width and height of cavity |
| $x, y$ | coordinate directions. |

Greek symbols

| | |
|---|---|
| $\alpha$ | dummy variable for integration |
| $\beta_s$ | solutal coefficient of volume expansion |
| $\beta_T$ | thermal coefficient of volume expansion |
| $\Gamma$ | generic diffusion coefficient |
| $\mu$ | dynamic viscosity |
| $\rho$ | density |
| $\phi$ | generic dependent variable |
| $\psi$ | streamfunction |

Superscripts/subscripts

| | |
|---|---|
| e | eutectic conditions |
| cold | conditions at cold wall |
| eff | effective value of transport coefficients for mushy fluid model |
| hot | conditions at hot wall |
| int | initial conditions |
| l | liquid phase |
| ref | reference conditions ($T_{ref} = T_e$ and $C_{ref} = C_e$) |
| s | solid phase |
| * | interface value. |

equations expressing mass, momentum, solute and energy transport have to be developed for each phase. At this stage it is important to emphasize the difference between a general formulation and a specific model. The development of the general transport equations accounting for the two-phase nature of the system is the formulation. The implementation of this formulation, on making various assumptions, results in a specific model. The reduction of a general two-phase formulation to specific models of binary alloy solidification systems is the approach adopted in the current work. It is noted that this approach of starting from a general two-phase formulation of a binary solidification system is also proposed and implemented in the work of Viskanta and Beckermann [24, 25].

In general the existing specific models of binary solidification systems are one-phase models in terms of 'averaged' or 'mixture' quantities [19–25]. In particular the specific one-phase model developed has been for a binary columnar dendritic alloy–mixture solidifying at local equilibrium conditions. Solidification systems, however, are diverse and as such there is not a unique set of assumptions for deriving a single limiting one-phase model. The application of specific assumptions will depend upon the exact physics of the situation to be modelled. The aim of this paper is to identify a range of physically meaningful assumptions under which a general two-phase description of a binary solidification reduces to a limiting one-phase model. In particular systems that do not involve a columnar dendritic structure (e.g. equiaxed or waxy materials), and or systems where the local equilibrium condition does not hold will be investigated. Essentially the questions to be answered are given below.

What are the possible assumptions which can be made in obtaining a limiting one-phase model?

What are the physical consequences of using such assumptions?

How does the performance of the resulting one-phase models differ?

## 2. A TWO-PHASE DESCRIPTION

A general two-phase description of a binary solidification system can be developed in the spirit of the well-known two-fluid model (e.g. see, Carver [26] and Ishii and Mishima [27]). The basic principal of the two-fluid approach is the development of separate governing equations for each phase (solid and liquid in the current case) which are then coupled through interphase transfer terms. For a solidifying binary system in two-dimensional Cartesian geometry, the

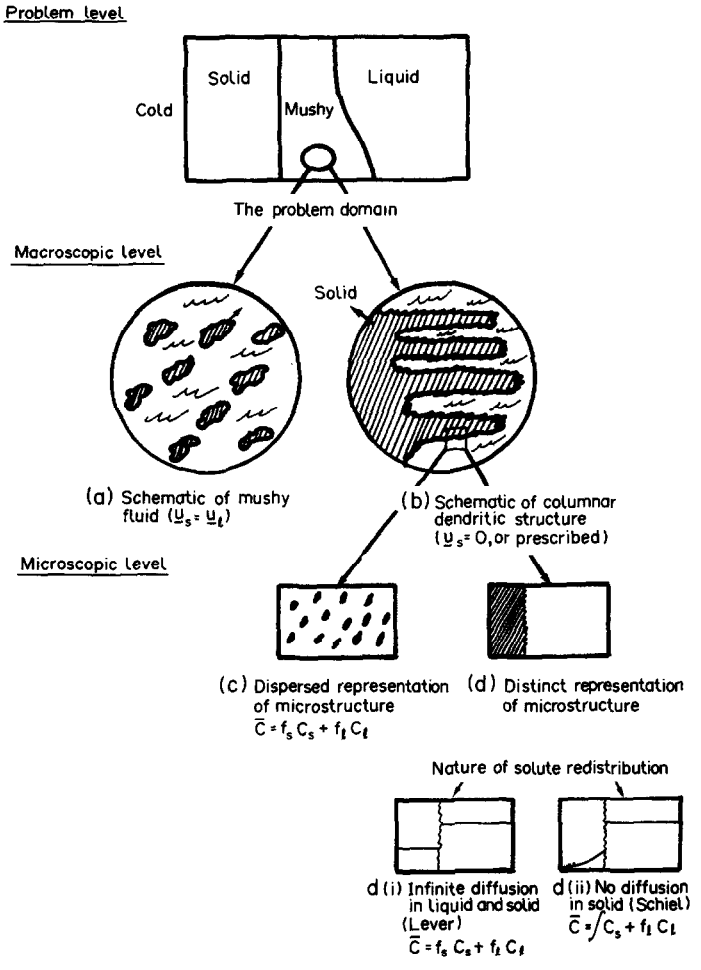


FIG. 1. The problem domain: (a) schematic of mushy fluid ($\mathbf{u}_s = \mathbf{u}_l$); (b) schematic of columnar dendritic structure ($\mathbf{u}_s = 0$, or prescribed); (c) dispersed representation of microstructure ($\bar{C} = f_s C_s + f_l C_l$); (d) distinct representation of microstructure; (d)(i) infinite diffusion in liquid and solid (Lever) ($\bar{C} = f_s C_s + f_l C_l$); (d)(ii) no diffusion in solid (Schiel) ($\bar{C} = \int C_s + f_l C_l$).

two-fluid model equations take the following general form:

$$\frac{\partial}{\partial t}(\rho_s g_s \phi_s) + \nabla \cdot (\rho_s g_s \mathbf{u}_s \phi_s) = \nabla \cdot (g_s \Gamma_s \nabla \phi_s) + \text{Source} + [\text{Interphase terms}] \quad (1)$$

$$\frac{\partial}{\partial t}(\rho_l g_l \phi_l) + \nabla \cdot (\rho_l g_l \mathbf{u}_l \phi_l) = \nabla \cdot (g_l \Gamma_l \nabla \phi_l) + \text{Source} - [\text{Interphase terms}] \quad (2)$$

for the solid and liquid phases, respectively, where $\phi_s$ and $\phi_l$ represent the values of any conserved (enthalpy, concentration, momentum) variables, the parameters $g_s$ and $g_l$ are the solid and liquid volume fractions in a representative region, $\mathbf{u}_s$ and $\mathbf{u}_l$ are the solid and liquid velocities, $\rho_s$ and $\rho_l$ the solid and liquid densities and, $\Gamma_s$ and $\Gamma_l$ are the solid and liquid diffusion coefficients, respectively. The volume fractions are related to the mass fractions, $f_s$ and $f_l$, by

$$\rho f_s = \rho_s g_s \quad \text{and} \quad \rho f_l = \rho_l g_l \quad (3)$$

where

$$\rho = \rho_s g_s + \rho_l g_l. \quad (4)$$

On setting the volume fractions to appropriate values in the solid, mushy and liquid regions, equations (1) and (2) will be valid throughout the domain of interest. The term Source represents effects not included in the main elements of the equation, e.g. dispersion fluxes and pressure gradients. Note that the interphase transfer terms have opposite signs and will cancel out in an additive combination of the phases. A detailed description can be developed from equations (1) and (2) on making the following substitutions.

Conservation of mass: $\phi$ is set to 1 and $\Gamma$ is set to 0.

Conservation of momentum: $\phi$ is set to a velocity component ($u_s$, $v_s$, $u_l$, and $v_l$) and $\Gamma$ is set to the viscosity $\mu$. A common pressure $P$ is shared between the phases,

and pressure gradient terms $-\partial P/\mathrm{d}x$ and $-\partial P/\mathrm{d}y$ are added to the $u$ and $v$ momentum equations, respectively.

Conservation of enthalpy: in the transient and convective terms $\phi$ is set to the total enthalpy, $H$. Neglecting solutal variations and assuming thermal equilibrium at the solid–liquid interface this leads to

$$H_s = \int_0^T c_s \,\mathrm{d}T, \quad H_l = \int_0^T c_l \,\mathrm{d}T + L \tag{5}$$

where $L$ is the latent heat of fusion and the $c$'s are specific heats. In the diffusion term $\phi$ is set to temperature $T$ and $\Gamma$ is the conductivity $K$.

Conservation of solute: $\phi$ is set to the mass fraction of solute species and $\Gamma$ is set to the species diffusion coefficient $D$.

## 3. MODELS WITH A ONE-PHASE FORM

### 3.1. *Basic assumptions*

To develop a one-phase model from the above two-phase equation set a number of assumptions and auxiliary relationships have to be invoked. The variables in one-phase models are usually the 'mixture' properties. The specification of the auxiliary relationships and identification of the variables will depend on the physics of the phase change in question and it is at this point that different one-phase models emerge.

The base line assumptions used in all the models presented here, consistent with previous studies [19–25], are: (i) Newtonian and laminar flow, (ii) homogeneous and isotropic properties in the phases, (iii) effects of small disturbances in the fields (e.g. dispersion fluxes, supercooling of the liquid, etc.) are neglected, and (iv) thermodynamic equilibrium at the solid–liquid interface (i.e. at the interface $T^* = T_s = T_l$ and $C_s^* = kC_l^*$). These assumptions will be extended and additional assumptions added as the various models are developed.

### 3.2. *A generic form*

The generic form of the governing equations for a one-phase model are given in Table 1. These equations are developed in terms of an enthalpy $h$, defined as

$$h = \int_0^T c_s \,\mathrm{d}T \tag{6}$$

and a system velocity

$$\rho\mathbf{u} = \rho_s g_s \mathbf{u}_s + \rho_l g_l \mathbf{u}_l. \tag{7}$$

Note that with this enthalpy definition $H_s = h$, $H_l = h + \delta H$ where

$$\delta H = \int_0^T (c_l - c_s) \,\mathrm{d}T + L \tag{8}$$

and $\nabla T = \nabla h / c_s$.

The definition of the generic parameters marked with a superscript $(\,)^+$ and the generic source terms $S_h$, $S_C$, $F_x$ and $F_y$ in Table 1 will depend on the model in question, i.e. the current set of assumptions. The various assumptions and hence the possible forms of these parameters, variables and sources are examined below.

Table 1. The general model

Mass

$$\frac{\partial}{\partial t}(\rho) + \nabla \cdot (\rho \mathbf{u}) = 0$$

Momentum

$$\frac{\partial}{\partial t}(\rho u) + \nabla \cdot (\rho \mathbf{u} u) = \frac{-\partial P}{\partial x} + \nabla \cdot (\mu^+ \nabla u) + F_x$$

$$\frac{\partial}{\partial t}(\rho v) + \nabla \cdot (\rho \mathbf{u} v) = \frac{-\partial P}{\partial y} + \nabla \cdot (\mu^+ \nabla v) + F_y - \rho g_r$$

Enthalpy

$$\frac{\partial}{\partial t}(\rho h) + \nabla \cdot (\rho \mathbf{u} h) = \nabla \cdot \left( \frac{K^+}{c_s} \nabla h \right) + S_h$$

Solute

$$\frac{\partial}{\partial t}(\rho C^+) + \nabla \cdot (\rho \mathbf{u} C^+) = \nabla \cdot (D^+ \nabla C^+) + S_C$$

### 3.3. *A comment on the scale*

In the numerical modelling of solidification systems it is important to recognize the large differences in scales upon which the various phenomena occur. The development of the transport equations takes place on the macroscopic scale with a number of computational cells being used to resolve the two-phase region. In typical applications these control volumes are of the order of $10^{-2}$ m. In many systems, however, the solid–liquid morphology is very fine, being of the order of 10–100 $\mu$m. If all solidification phenomena are to be fully accounted for, the effect of the solid–liquid morphology cannot be ignored. Essentially any macroscopic analysis needs to 'capture' the influences of the phenomena that occur on the microscopic scale [28].

### 3.4. *Two limiting cases*

On the macroscopic level, in deriving one-phase models, two limiting cases can be identified. Case 1 in which the solid is fully dispersed in the liquid phase and the solid and liquid velocities are equal (Fig. 1(a)). Case 2 in which the solid matrix is distinct from the liquid and the matrix is either fixed (i.e. $\mathbf{u}_s = 0$) or moves with a prescribed velocity (Fig. 1(b)). Both of these cases have physical relevance, lead to governing equations with a one-phase form, and result in models which can be implemented using standard numerical solution schemes for elliptic equations [29].

### 3.5. *The mushy fluid model (Model A)*

This model is applicable to amorphous materials (e.g. waxes and glasses) and in a limited sense, the

equiaxed zone of a metal casting. In the mushy fluid model, the solid is assumed to be fully dispersed within the liquid and moving with the same velocity, i.e.

$$\mathbf{u} = \mathbf{u}_s = \mathbf{u}_l. \tag{9}$$

The nature of the mushy fluid model is illustrated in Fig. 1(a). Using the given velocity assumption, equation (9), along with the enthalpy, $h$, and system velocity, $\mathbf{u}$, the two-fluid equations can be combined to eliminate the interphase transfer terms. The appropriate one-phase parameters and source terms that result from this step are summarized in Table 2(a). In relation to this model the following comments are made.

In the development of the model it is convenient to assume effective diffusion coefficients as the average of the single phase coefficients, e.g. $\mu_{\text{eff}} = \mu_s g_s + \mu_l g_l$.

On considering the conservation of solute it is recognized that within the mushy fluid mushy region, all parts of the solid are in equilibrium with the surrounding fluid. Essentially the solid–liquid interface is distributed throughout the mushy region and the concentration of solute in the liquid and solid phases will be related via $C_s = kC_l$. Hence the solute transport can be expressed in terms of the solute concentration, i.e. $C^+ = C_s$, resulting in the solute equation of Table 1 with Source term $S_C$ defined in Table 2(a). Note that as an alternative the solute equations can be written in terms of a mixture concentration defined by $C_{\text{mix}} = f_l C_l + f_s C_s$.

The central requirement in an implementation of the mushy fluid model is that the *system* velocity approaches to zero as the local liquid fraction nears zero, i.e. there is no velocity in a full solid region. In practical cases this reduction in velocity can be achieved by specifying a large solid viscosity, $\mu_s$. Then, provided no isolated regions or 'islands' of full solid develop, as $g_s$ tends to unity the value of $\mu_{\text{eff}}$ will increase and dominate the momentum equations, finally extinguishing the velocity $\mathbf{u}$ upon full solidification.

### 3.6. *Columnar dendritic with dispersed microstructure (Model B)*

In this model the solid phase is assumed to be distinct from the liquid and moving with a prescribed velocity (zero in a static casting or nonzero in continuous casting). In a physical sense this model approximates the columnar dendritic zone of a solidifying metallurgical alloy. A descriptive illustration of the nature of the columnar dendritic zone is shown in Fig. 1(b). Note that for the static casting system ($u_s = 0$) the system velocity is given by $\rho\mathbf{u} = \rho_l g_l \mathbf{u}_l$. For clarity, only cases in which the prescribed velocity is zero will be considered in the following analysis.

The assumption of a dendritic structure is made on the macroscopic scale. On the microscopic scale the manner in which the microstructure is represented has an important effect on the resulting model. Two versions of the columnar dendritic model will be considered. In the first version the microstructure will be modelled as a dispersed solid in a liquid matrix (Fig. 1(c)).

The definitions of the generic parameters and source terms, defined in Table 1, which are appropriate for the columnar dendritic dispersed microstructure model, are given in Table 2(b). A discussion of this model now follows.

The mass and enthalpy transport equations are derived by adding the appropriate two-fluid equations and setting $\mathbf{u}_s = 0$ in each case. In deriving the momentum equations it is tempting to directly combine the two-fluid momentum equations. However, if such an approach is used, care must be taken to avoid any inconsistency in the definition of the pressure which, in the two-fluid model, is taken to be the same in each phase. In the current model this potential problem is avoided on adopting the approach proposed by Bennon and Incropera [20–23]. It is recognized that in order to prescribe the solid velocity, $\mathbf{u}_s$, an external force $\mathbf{F}(F_x, F_y)$, needs to be introduced to ensure that the two-phase solid momentum equations are well defined so that they can be combined with the liquid phase equations. An appropriate expression for $\mathbf{F}$ may be found by appealing to the nature of the flow in the mushy region, which in the case of a columnar dendritic structure is governed by the Darcy law [30]. The forms for $F_x$ and $F_y$, given in Table 2(b), are derived on applying the Carman–Kozeny equation for flow in a porous media [18, 20–23]. Using the given definition of $F$, adding the two-fluid momentum equations and applying the additional assumptions, (i) a solid free of internal stress, (ii) small viscous stresses resulting from local density gradients, and (iii) a constant density in each phase [20–23], will result in the required one-phase momentum equations given in Tables 1 and 2(b). The following observations on these momentum equations are pertinent.

(1) The momentum equations are identical to those proposed by Bennon and Incropera (equation (26) in ref. [20]). With the additional conditions of a zero solid velocity and constant density, these equations reduce to the momentum equations proposed in ref. [18].

(2) The source terms ($F_x$ and $F_y$) become zero in the full liquid regions and override the other terms in the mushy region to force the momentum equations to mimic the Carman–Kozeny equations.

(3) An alternative to using the prescribed force approach [20–23] is to develop an appropriate equation from the liquid phase alone [24, 25].

In the columnar dendritic models the one-phase transport of the solute equation is derived directly on considering a macroscopic solute balance in an arbitrary fixed control volume within the mushy region. From such a balance the following equation can be derived [24, 25, 31]:

Table 2. (a) Model A, the mushy fluid model; (b) Model B, columnar dendritic with dispersed microstructure ($\mathbf{u}_s = 0$); (c) Model C, columnar dendritic with distinct microstructure ($\mathbf{u}_s = 0$)

| | (a) | (b) | (c) |
|---|---|---|---|
| *Parameters* | | | |
| System velocity | $\mathbf{u} = \mathbf{u}_l = \mathbf{u}_s$ | $\mathbf{u} = f_l\mathbf{u}_l$ | $\mathbf{u} = f_l\mathbf{u}_l$ |
| Concentration | $C^+ = C_s$ | $C^+ = C_s$ | $C^+ = C_l$ |
| Viscosity | $\mu^+ = \mu_{eff} = \mu_s g_s + \mu_l g_l$ | $\mu^+ = \mu_l \rho/\rho_l$ | $\mu^+ = \mu_l \rho/\rho_l$ |
| Solute diffusion | $D^+ = \rho_s g_s D_s + \rho_l g_l D_l/k$ | $D^+ = \rho_s g_s D_s + \rho_l g_l D_l/k$ | $D^+ = \rho_l g_l D_l$ |
| Thermal diffusion | $K^+ = g_s K_s + g_l K_l$ | $K^+ = g_s K_s + g_l K_l$ | $K^+ = g_s K_s + g_l K_l$ |
| *Source terms* | | | |
| Momentum | $F_x = 0$ | $F_x = -\{K_0(1-g_l)^2/g_l^3(\rho/\rho_l)\}u$ | $F_x = -\{K_0(1-g_l)^2/g_l^3(\rho/\rho_l)\}u$ |
| | $F_y = 0$ | $F_y = -\{K_0(1-g_l)^2/g_l^3(\rho/\rho_l)\}v$ | $F_y = -\{K_0(1-g_l)^2/g_l^3(\rho/\rho_l)\}v$ |
| Enthalpy | $S_h = \dfrac{-\partial}{\partial t}(\rho f_l \delta H) - \nabla\cdot(\rho f_l \mathbf{u}\delta H)$ | $S_h = \dfrac{-\partial}{\partial t}(\rho f_l \delta H) - \nabla\cdot(\rho \mathbf{u}\delta H)$ | $S_h = \dfrac{-\partial}{\partial t}(\rho f_l \delta H) - \nabla\cdot(\rho \mathbf{u}\delta H)$ |
| Solute | $S_C = \dfrac{-\partial}{\partial t}[(1/k-1)\rho f_l C_s] - \nabla\cdot[(1/k-1)\rho f_l \mathbf{u} C_s]$ | $S_C = \dfrac{-\partial}{\partial t}[(1/k-1)\rho f_l C_s] - \nabla\cdot[(1/k-1)\rho \mathbf{u} C_s]$ | $S_C = \dfrac{\partial}{\partial t}(\rho(1-f_l)C_l) - \rho k C_l \dfrac{\partial(\rho f_s)}{\partial t}$ |
| Temperature—solute coupling | $T = \dfrac{T_L - (1-f_l)(1-k)T_m}{[1-(1-f_l)(1-k)]}$ | $T = \dfrac{T_L - (1-f_l)(1-k)T_m}{[1-(1-f_l)(1-k)]}$ | $T = T_m - (T_m - T_e)C_l/C_e$ |
| | $T_L = T_m - (T_m - T_e)C_{mix}/C_e$ | $T_L = T_m - (T_m - T_e)C_{mix}/C_e$ | |

$$\frac{\partial}{\partial t}(\rho C_{mix}) + \nabla \cdot (\rho \mathbf{u} C_l) = \nabla \cdot (\rho_s g_s D_s \nabla C_s + \rho_l g_l D_l \nabla C_l) \tag{10}$$

where $C_{mix}$ is a representative value obtained by space averaging over a volume defined on the microscopic scale (see Fig. 1(b)). On a conceptual level this microscopic volume can be considered to be similar to the 'volume probe' used in the two-phase analysis of gas–particle aggregates [32]. Representing this microscopic volume by $V = V_s$ (volume of the solid fraction) + $V_l$ (volume of the liquid fraction), the general form of $C_{mix}$ can be written as

$$C_{mix} = \frac{\int \rho_l C_l \, dV_l + \int \rho_s C_s \, dV_s}{\rho V}. \tag{11}$$

The assumed nature of the microstructure and solute redistribution mechanisms in the microscopic volume will determine the exact form of $C_{mix}$. In the case of a dispersed microstructure (Fig. 1(c)) the solid matrix is assumed to be dispersed throughout the liquid and $C_{mix} = f_l C_l + f_s C_s$ with $C_s = kC_l$ at all points inside the mushy region. Hence the solute conservation, equation (10), can be written in the one-phase form with the $C^+$, $D_{eff}$, and $S_C$ as defined in Table 2(b).

### 3.7. *Columnar dendritic with distinct microstructure (Model C)*

On the macroscopic scale this model is identical to Model B (Table 2(b)), i.e. the mushy region consists of an array of columnar dendrites as depicted in Fig. 1(b). The microstructure, however, is represented as a distinct solid and liquid region (Fig. 1(d)). This may be seen as the opposite extreme to a dispersed microstructure (Fig. 1(c)). The definitions appropriate to this model are given in Table 2(c). The mass, momentum and enthalpy transport equations are identical to the previous model presented, Model B (Table 2(b)). It is in the solute transport equation where differences arise, in particular the manner in which $C_{mix}$ (equation (11)) is calculated. The form of $C_{mix}$ in the current model will depend on the assumed local solute transport mechanisms on the microscopic scale. In a metallurgical context there are two alternative situations which can be considered.

(1) Diffusion of solute, on the microscopic scale, is assumed to be infinite in both the solid and the liquid (i.e. the Lever rule applies) resulting in uniform concentration profiles (Fig. 1(d)(i)). This means that all parts of the solid are in equilibrium with all parts of the liquid and conditions are essentially the same as those found in a dispersed microstructure, i.e. Model B (Table 2(c)).

(2) Diffusion in the liquid is infinite and diffusion in the solid is zero. This is the assumption upon which the Scheil equation is based. The Scheil equation is valid in many metallurgical solidification situations [33]. In this case the solute concentration in the liquid will be uniform, whereas the solute concentration in the solid will have a profile (Fig. 1(d)(ii)). The Scheil approach is explored below.

On noting that $V_s = g_s V$, equation (11) takes the form

$$\rho C_{mix} = \rho f_l C_l + \int_0^{g_s} C_s \, d\alpha \tag{12}$$

where $\alpha$ is a dummy variable for carrying out the integration. Under the assumption of no local remelting, since there is no transport of solute within the solid, the concentration at any point in the solid remains equal to the concentration when the solid first formed. The integrand in the second term on the right-hand side of equation (12) is therefore independent of time. Furthermore, when $\alpha = g_s(t)$, the current position of the solid front has been reached and $C_s = C_s^* = kC_l$. Using these observations and applying Leibnz's rule, leads to the following relationship (see Appendix):

$$\frac{\partial(\rho C_{mix})}{\partial t} = \frac{\partial}{\partial t}(\rho C_l) + \frac{\partial}{\partial t}(\rho(f_l - 1)C_l) + kC_l \frac{\partial}{\partial t}(\rho f_s). \tag{13}$$

Substituting this expression into the solute conservation equation (equation (10)), along with the assumption of zero diffusion in the solid, leads to the appropriate terms for $D^+$ and $S_C$ given in Table 2(c).

### 3.8. *Coupling*

Before the various models developed above can be numerically resolved, an auxiliary relationship needs to be defined for coupling the enthalpy (temperature) and solute fields. The temperature–solute coupling relationships for each of the models are given in Tables 2(a)–(c). The form of these models depends on the nature of the assumptions used.

In the case of a mushy fluid (Model A), a dispersed microstructure (Model B), and a distinct microstructure with local thermodynamic equilibrium (equivalent to Model B), this coupling is achieved through the equilibrium phase change diagram for the binary system in question (Fig. 2). On assuming straight liquidus and solidus lines in the phase diagram, the relationships given in Tables 2(a) and (b) can be obtained by simple geometry.

In the case of a distinct microstructure (Model C), equilibrium does not exist throughout a microscopic volume and a non-equilibrium treatment of the coupling is therefore required. On making the assumption that the temperature of a microscopic volume changing phase is at the liquidus temperature, $T_L$, corresponding to the current liquidus concentration, $C_l$, the temperature at any point in the mushy region can be related to the liquid concentration via the liquidus line of the phase change diagram (Fig. 2). This is the basis for the coupling relationship given in Table 2(c).

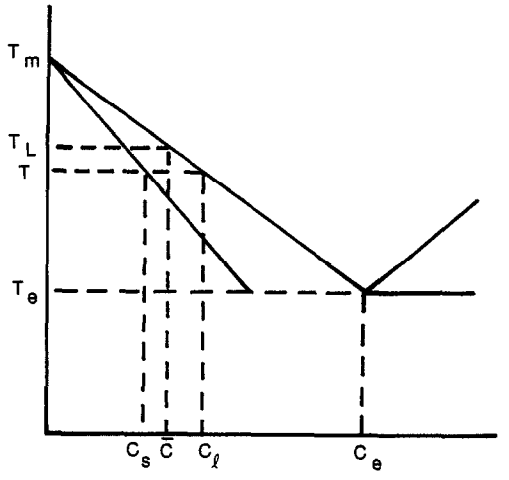


FIG. 2. The phase change diagram.

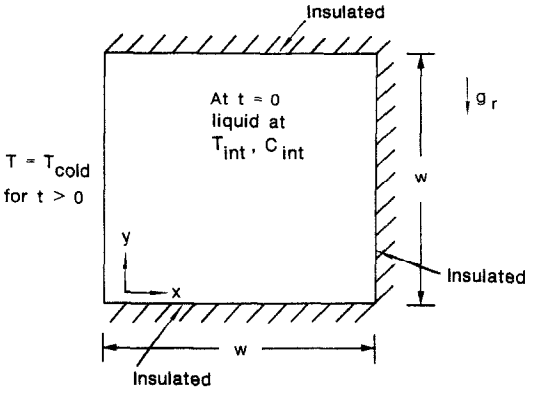


FIG. 3. Schematic diagram of the test problem.

3.9. *Summary*

At this point it is worthwhile to place in context, with the previous work, the one-phase models outlined in Tables 1 and 2.

Model A (the mushy fluid model). The effective viscosity term introduced in the momentum equations has been suggested by many previous investigators [14, 15, 20, 24]. The current authors, however, are unaware of any previous attempts to develop solute and enthalpy transport equations based on the mushy fluid model.

Model B (the columnar dendritic model) with dispersed microstructure. This model is essentially equivalent to the one-phase model investigated in previous studies [19–25]. A feature of this model is the assumption of local thermodynamic equilibrium. This requires that on the microscopic scale, either the solid solute diffusion is infinite (Lever rule) or the solid is fully dispersed in the liquid. Both of these additional assumptions are in conflict with the assumed macroscopic nature of a columnar zone (i.e. small if not zero solid solute diffusion and distinct solid and liquid regions).

Model C (the columnar dendritic model with distinct microstructure). In many respects this model is similar to the previous dendritic model, Model B. In this case, however, local solute equilibrium is not assumed. The solute transport mechanism is based on a distinct microstructure with the assumption of zero solid solute diffusion (the Scheil approach). Such an approach is closer to the underlying physics of a columnar zone. The authors are unaware of any previous attempts to include a non-equilibrium treatment into a one-phase model of a binary solidification.

## 4. PRELIMINARY RESULTS AND NUMERICAL INVESTIGATIONS

4.1. *The test problems*

In this section results of a number of numerical experiments will be discussed in order to highlight the differences between the models. The test problem is as described in Section 1.1, the geometry is given in Fig. 3. Full problem specifications are given in Table 3. The thermophysical data used in this problem approximate an aqueous ammonium chloride solution. The Boussinesq approximation is used and hence the term $\rho g_r$ appearing in the momentum equations can, after appropriate redefinition of the pressure, be replaced by

$$\rho_{\text{ref}} g_r [\beta_T (T - T_e) + \beta_s (C_l - C_e)] \qquad (14)$$

where $\rho_{\text{ref}}$ is a reference density existing at $T = T_e$ and $C = C_e$.

In all the computations a space grid of $30 \times 30$ and a variable time step of 1–25 s (chosen to ensure small changes in the liquid fraction) were used. Iterations for each time step were terminated when the residual mass source within each control volume fell below $8 \times 10^{-6}$ and the error in an overall energy and solute balance dropped below $1 \times 10^{-2}$ and $1 \times 10^{-4}$%, respectively. For a simulation spanning 3000 s, approximately 20 CPU min were required on a Cray 2 computer.

4.2. *Numerical scheme*

The emphasis in this paper focuses on comparing predictions from the various one-phase models outlined in Table 2. Only a brief account of the numerical implementation of the models is given. The numerical scheme used is based on a control-volume formulation and the SIMPLE algorithm is applied to resolve the pressure–velocity coupling [29]. Treatment of the phase change is based on the approach proposed in ref. [18]. The essential feature is the iteration of the local liquid fraction field until the predicted enthalpy and solute fields are in agreement according to the given temperature–solute relationship. Full details of this procedure have been recently reported [35]. With a grid of $30 \times 30$ a full resolution of all the phenomena is probably not possible. It is felt, however, that the grid is sufficient to resolve the major qualitative features of the models in question and thereby fulfil the basic aim of the current work.

Table 3. Data for test problem (aqueous ammonium chloride solution)

| | |
|---|---|
| *Initial and boundary conditions* | |
| Cavity dimensions | $w = 0.025$ m |
| Initial liquid concentration | $C_{int} = 0.1$ kg m$^{-3}$ |
| Initial temperature | $T_{int} = 600$ K |
| Left wall temperature for $t > 0$ | $T_{cold} = 400$ K |
| *Thermophysical properties* | |
| Specific heat | $c = 3000$ J kg$^{-1}$ K$^{-1}$ |
| Thermal conductivity | $K = 0.4$ W m$^{-1}$ K$^{-1}$ |
| Density | $\rho = 1000$ kg m$^{-3}$ |
| Liquid viscosity | $\mu_l = 1.0 \times 10^{-3}$ kg m$^{-1}$ s$^{-1}$ |
| Solid viscosity | $\mu_s = 1 \times 10^{4}$ kg m$^{-1}$ s$^{-1}$ |
| Species diffusion coefficient | $D = 4.8 \times 10^{-9}$ m$^2$ s$^{-1}$ |
| Latent heat | $L = 3 \times 10^{5}$ J kg$^{-1}$ |
| Permeability coefficient | $K_0 = 2 \times 10^{6}$ kg m$^{-3}$ s$^{-1}$ |
| Thermal expansion coefficient | $\beta_T = 4 \times 10^{-5}$ K$^{-1}$ |
| Solutal expansion coefficient | $\beta_s = 0.025$ |
| Eutectic temperature | $T_e = 250$ K |
| Eutectic concentration (mass fraction) | $C_e = 0.8$ |
| Melting point of pure material | $T_m = 630$ K |
| Equilibrium partition ratio | $k = 0.3$ |

There are many features of binary solidification systems worth investigating using any one of the one-phase models. The ultimate aim of a modelling analysis, however, is to predict patterns of macro-segregation. As such this is chosen as the point of comparison in the present study.

4.3. *Evolution of macro-segregation*

Macro-segregation arises as a result of the convective redistribution of solute rejected by solidifying material. The final pattern of macro-segregation predicted will therefore be intimately linked to the flow field history of the solidification process. The flow is a thermo-solutal driven flow, i.e. the driving force for flow includes both thermal and concentration gradient terms (see equation (14)). Thermal influences would be expected to govern flow at early times when high temperature gradients exist and the fluid composition is uniform and close to the initial concentration. As solidification proceeds, however, the thermal gradients decay and solute concentration gradients appear as a result of macro-segregation effects.

A typical development of the thermo-solutal driven flow field may be studied by examining Fig. 4 in which the streamlines and the $f_l = 0.5$ contour are plotted for Model B at $t = 100$, 250 and 500 s, respectively. At 100 s (Fig. 4(a)) a strong counterclockwise flow field is generated by the high thermal gradients which arise immediately after lowering the left-hand wall to $T_{cold} = 400$ K from the initial temperature of 600 K. After 250 s, however, the thermal gradients have diminished considerably and significant solute gradients have arisen. In Fig. 4(b) it can be seen that at $t = 250$ s a small, clockwise recirculation cell ($\psi_{min} = -2 \times 10^{-4}$) driven by solute concentration gradients appears at the lower left of the main circulation zone ($\psi_{max} = 1.3 \times 10^{-3}$). This solutal driven recirculation cell results from the steep concentration gradients near the base of the cavity, concentration gradients created by the 'washing' of the mushy region by the counterclockwise thermal flow at early solidification. As time progresses and temperature gradients continue to decay, solutal influences begin to dominate over thermal buoyancy effects. After $t = 500$ s, the circulation pattern is totally reversed and only a single, solutal driven circulation zone exits (Fig. 4(c)).

4.4. *The macro-segregation*

The complex flow fields arising from the competing thermal and solute concentration buoyancy forces, along with the modelling assumptions used to describe the mushy region, determine the final macro-segregation patterns predicted. The mean solute concentration fields at $t = 3000$ s obtained when using the mushy fluid model (Model A), the columnar dendritic model with a dispersed microstructure (Model B) and the columnar dendritic model with a distinct microstructure (Model C) are illustrated in Fig. 5 by selected iso-concentration contours.

Figure 5(a) shows the macro-segregation pattern predicted by the mushy fluid model (Model A) at $t = 3000$ s, using a solid viscosity of $\mu_s = 1 \times 10^4$. After solidification is initiated, thermally induced flow in the mushy and full liquid regions arises in an anticlockwise direction (similar to that shown in Fig. 4). As the phase change proceeds, solute is rejected from the solid fraction into the liquid. However, as the solid moves along with the fluid in this model ($\mathbf{u}_l = \mathbf{u}_s$) differences are smoothed out and the steep concentration gradients associated with the columnar dendritic models (in which the solid is stationary), do not arise. Hence, the flow in the cavity is driven solely by thermal buoyancy influences throughout the solidification process. The result is a final macro-seg-

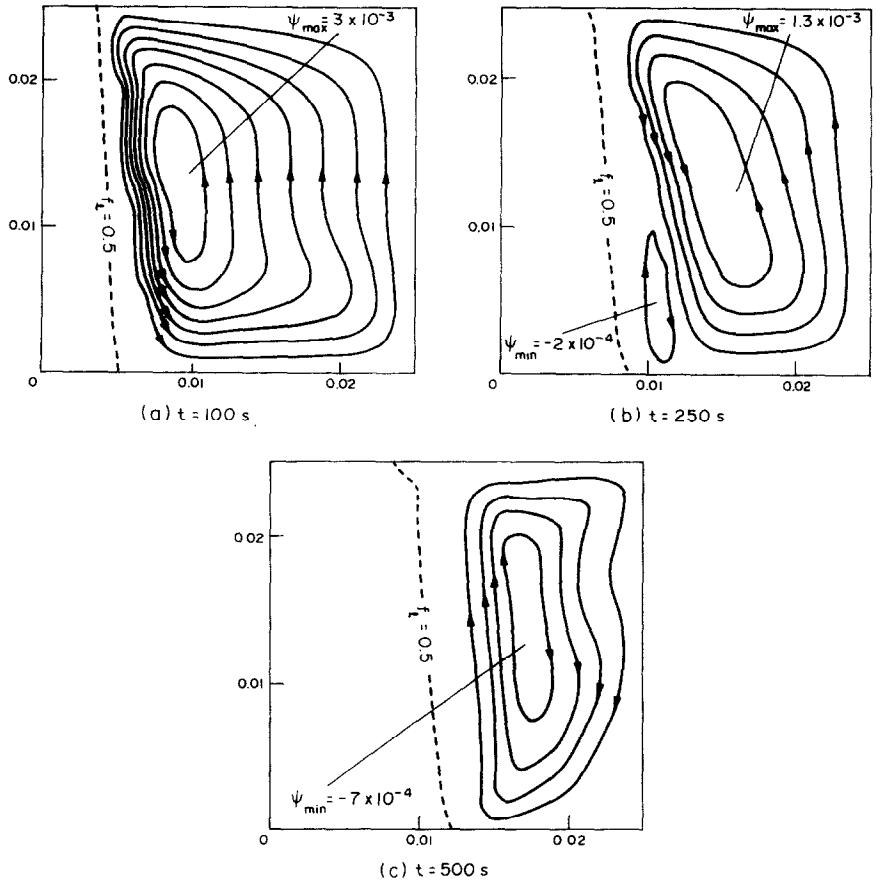


FIG. 4. Streamlines and $f_l = 0.5$ contours at: (a) $t = 100$ s; (b) $t = 250$ s; (c) $t = 500$ s.

regation pattern (Fig. 5(a)), in which rejected solute has been preferentially deposited in the lower region of the cavity.

The qualitative behavior of the macro-segregation patterns obtained from Models B and C are similar (Figs. 5(a) and (b)). In particular, the areas of large positive segregation are located along the right of the upper walls. This is a result of the solutal buoyancy flow dominating the later stages of solidification. This flow causes light fluid, rich in solute, to rise to the top of the cavity as solidification progresses and solute is rejected into the liquid phase.

As for the differences between the models, the segregation predicted by Model C (distinct microstructure) is more severe ($C_{mix} = 0.06$–$0.25$) than that predicted by Model B (dispersed microstructure) ($C_{mix} = 0.07$–$0.21$). In particular, in the dispersed microstructure model the bulk of the cavity is close to the nominal composition (0.1) whereas with the distinct microstructure there is a definite area of negative segregation (0.08).

Another point of difference between the columnar models, not explicitly indicated in Fig. 5, is the fact that with Model C full solidification does not occur at a point in the cavity. The reason for this behavior can be explained as follows. As the liquid fraction decreases, system velocities become small and 'pockets' of liquid become 'trapped' in the mushy region. Due to the nature of the microscopic solute redistribution assumed in the distinct microstructure model, the solute concentration in these pockets will increase. In the absence of other constraints, the concentration will increase to the eutectic, $C_e$, at which point the solidification would proceed as an isothermal phase change at the eutectic temperature, $T_e = 250$ K. In the current problem, however, the cold wall boundary condition, $T_{cold} = 400$ K, is well above the eutectic, $T_e = 250$ K, and solidification cannot be completed. If the cold wall temperature was taken below the eutectic temperature it would be expected that with Model C (distinct microstructure), on complete solidification, material with a eutectic composition would be predicted within every microscopic volume. In many columnar dendrite structures this behavior is physically reasonable in that material of the eutectic composition will form in the inter-dendritic spaces (see Fig. 6.4 in Flemings [33]).

### 4.5. *Summary*

In terms of the macro-segregation patterns predicted, the main points arising from the above analysis are as follows.

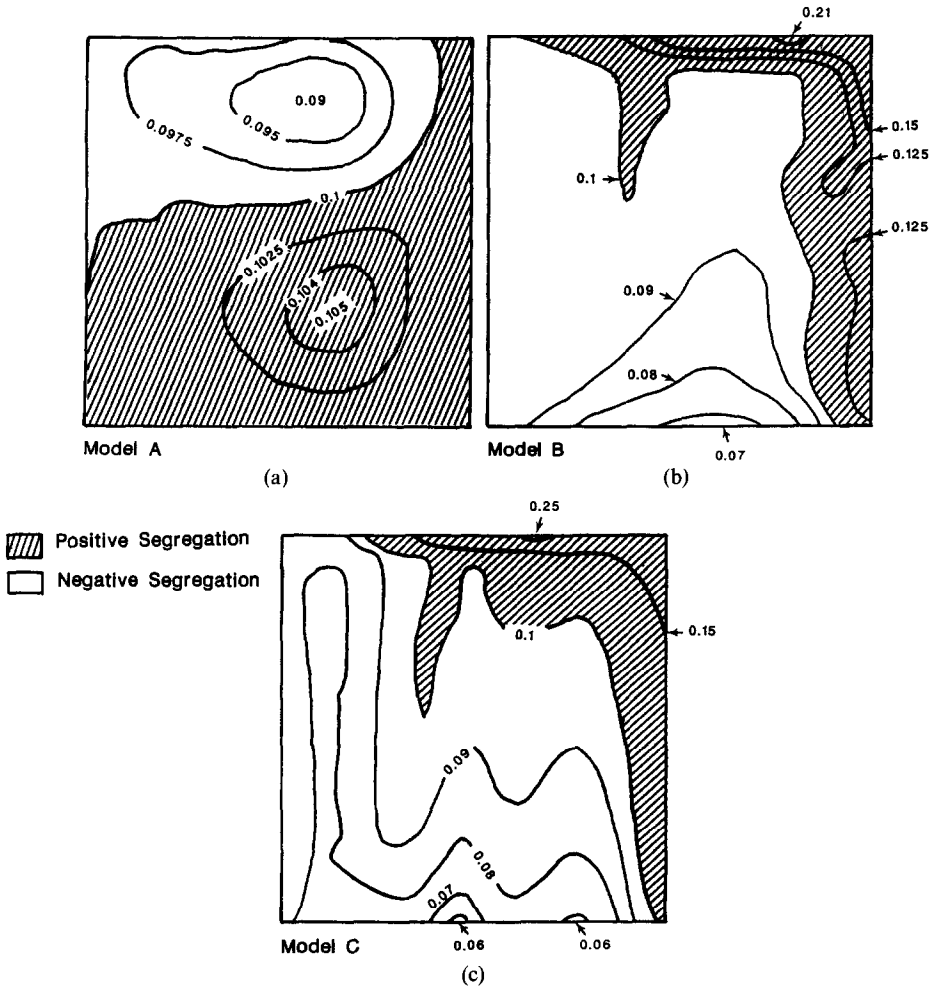


FIG. 5. Macro-segregation patterns at $t = 3000$ s: (a) Model A; (b) Model B; (c) Model C.

(1) Competing thermo-solutal buoyancy influences result in complex flow fields during the solidification process. These flow fields, along with the assumptions about the nature of the mushy region, dictate the final macro-segregation patterns predicted.

(2) Due to the fact that solid is convected in the mushy region, the mushy fluid model, Model A, predicts a macro-segregation pattern of a more uniform nature than the columnar dendritic models.

(3) With the columnar models the segregation predicted by Model C (distinct) is more severe than that predicted by Model B (dispersed).

(4) In using the columnar dendritic model with a distinct microstructure (Model C), complete solid will not form unless the wall temperature $T_{cold}$ is below the eutectic temperature. Upon complete solidification, on the microscopic scale, material at the eutectic composition will be predicted throughout the columnar region. This result is consistent with observations in many metallurgical systems [33].

## 5. CONCLUSIONS

On making various assumptions about the nature of binary solidification systems, three models with a one-phase form have been derived. The assumptions about the nature of the phase change are summarized in Fig. 1 and the governing equations of the derived models, mushy fluid (Model A), dispersed columnar (Model B) and distinct columnar (Model C) are given in Tables 1 and 2. The performance of the models in predicting macro-segregation patterns are illustrated in Fig. 5.

The concepts in the mushy fluid model (Model A) have been expressed elsewhere, but to the authors' knowledge a full set of governing equations has not been derived before. The dispersed columnar model (Model B) is similar to previous models of binary systems [19–25]. The distinct columnar model (Model C) is an important extension in that it allows for a non-equilibrium treatment and better approximates the microscopic physics. In a metallurgical context the mushy fluid model (Model A) could be valid for an analysis of solidification in the equiaxed zone. The columnar dendritic models (Models B and C) can be used to model the behavior in the columnar zone. In a true metallurgical system there will be a transition from an equiaxed to a columnar dendritic structure, and it would be expected that a hybrid of all the models presented here would be required in any full analysis.

*Acknowledgements*—C. Prakash's participation in this research was made possible by a Small Business Innovative Research Grant from NASA–Lewis (Contract No. NASA-25331; contract manager Dr Arnon Chait). A. D. Brent was funded by a Doctoral Dissertation Fellowship from the Graduate School of the University of Minnesota. The support by NASA–Lewis and the Graduate School of the University of Minnesota is gratefully acknowledged. Computations were carried out on an AT&T 3b2/400 microcomputer and a Cray 2. The support by both AT&T Information Systems, Inc. and the Minnesota Supercomputer Institute is gratefully acknowledged. The authors would also like to thank their colleagues who reviewed earlier versions of the manuscript. In particular Dr M. Rappaz of EPFL and Dr C. Beckermann of the University of Iowa.

## REFERENCES

1. N. R. Eyres, D. R. Hartree, J. Ingham, R. Jackson, R. J. Sarjant and J. B. Wagstaff, The calculation of variable heat flow in solids, *Phil. Trans. R. Soc.* **240(A),** 1–57 (1946).
2. M. C. Flemings and G. E. Nereo, Macro-segregation: Part I, *Trans. TMS–AIME* **239,** 1449–1461 (1967).
3. M. C. Flemings, R. Mehrabian and G. E. Nereo, Macro-segregation: Part II, *Trans. TMS–AIME* **242,** 41–49 (1968).
4. M. C. Flemings and G. E. Nereo, Macro-segregation: Part III, *Trans. TMS–AIME* **242,** 50–55 (1968).
5. R. Mehrabian, M. Keane and M. C. Flemings, Interdendritic fluid flow and macro-segregation, influence of gravity, *Metall. Trans. B* **1B,** 3228–3241 (1970).
6. S. Kou, D. R. Poirier and M. C. Flemings, Macro-segregation in electroslag remelted ingots, *Proc. Elect. Furn. Conf. Iron Steel Soc. AIME* **35,** 221–228 (1977).
7. A. L. Maples and D. R. Poirier, Convection in the two-phase zone of solidifying alloys, *Metall. Trans. B* **15B,** 163–172 (1984).
8. J. Crank, *Free and Moving Boundary Problems*. Clarendon Press, Oxford (1984).
9. T. W. Clyne, Modelling of heat flow in solidification, *Mater. Sci. Engng* **65,** 111–124 (1984).
10. E. M. Sparrow, S. V. Patankar and S. Ramadhyani, Analysis of melting in the presence of natural convection in the melt region, *J. Heat Transfer* **99,** 520–526 (1977).
11. A. Gadgil and D. Gobin, Analysis of two-dimensional melting in rectangular enclosures in presence of convection, *J. Heat Transfer* **106,** 20–26 (1984).
12. C. Benard, D. Gobin and A. Zanoli, Moving boundary problem: heat conduction in the solid phase of a phase-change material during melting driven by natural convection in the liquid, *Int. J. Heat Mass Transfer* **29,** 1669–1681 (1986).
13. J. Yoo and B. Rubinsky, A finite element method for the study of solidification processes in the presence of natural convection, *Int. J. Numer. Meth. Engng* **23,** 1785–1805 (1986).
14. K. Morgan, A numerical analysis of freezing and melting with convection, *Comp. Meth. Appl. Engng* **28,** 275–284 (1981).
15. V. R. Voller, M. Cross and N. C. Markatos, An enthalpy method for convection/diffusion phase change, *Int. J. Numer. Meth. Engng* **24,** 271–284 (1987).
16. A. D. Brent, V. R. Voller and K. J. Reid, The enthalpy porosity technique for modelling convection–diffusion phase change: application to the melting of a pure metal, *Numer. Heat Transfer* **13,** 297–318 (1988).
17. J. Szekely and A. S. Jassal, An experimental and analytical study of the solidification of a binary dendritic system, *Metall. Trans. B* **9B,** 389–398 (1978).
18. V. R. Voller and C. Prakash, A fixed grid numerical modelling methodology for convection–diffusion mushy region phase-change problems, *Int. J. Heat Mass Transfer* **30,** 1709–1720 (1987).
19. V. R. Voller, A numerical method for analysis of solidification in heat and mass transfer systems. In *Numerical Methods in Thermal Problems V* (Edited by R. W. Lewis *et al.*), pp. 693–704. Pineridge, Swansea (1987).
20. W. D. Bennon and F. P. Incropera, A continuum model for momentum, heat and species transport in binary solid–liquid phase change systems—1. Model formulation, *Int. J. Heat Mass Transfer* **30,** 2161–2170 (1987).
21. W. D. Bennon and F. P. Incropera, A continuum model for momentum, heat and species transport in binary solid–liquid phase change systems—2. Application to solidification in a rectangular cavity, *Int. J. Heat Mass Transfer* **30,** 2171–2187 (1987).
22. W. D. Bennon and F. P. Incropera, The evolution of macro-segregation in statically cast binary ingots, *Metall. Trans. B* **18B,** 611–616 (1987).
23. W. D. Bennon and F. P. Incropera, Numerical analysis of binary solid-liquid phase change using a continuum model, *Numer. Heat Transfer* **13,** 277–296 (1988).
24. R. Viskanta and C. Beckermann, Mathematical modelling of solidification. Presented at Symposium on 'Interdisciplinary Issues in Materials Processing and Manufacturing', ASME Annual Meeting, Boston, Massachusetts, 14–18 December (1987).
25. C. Beckermann and R. Viskanta, Double-diffusive convection during dendritic solidification of a binary mixture, *PCH* **10,** 195–213 (1988).
26. M. B. Carver, Numerical computation of phase separation in two fluid flow, *J. Fluids Engng* **106,** 147–153 (1984).
27. M. Ishii and K. Mishima, Two-fluid model and hydrodynamic constitutive relations, *Nucl. Engng Des.* **82,** 107–126 (1984).
28. M. Rappaz, Micro-/macroscopic modeling of solidification, *Int. Mater. Rev.* (1989), submitted.
29. S. V. Patankar, *Numerical Heat Transfer and Fluid Flow*. Hemisphere, Washington, DC (1980).
30. D. R. Poirier, Permeability for flow of interdendritic liquid in columnar-dendritic alloys, *Metall. Trans. B* **18B,** 245–256 (1987).
31. M. Rappaz and V. R. Voller, A note on accounting for the effect of the microstructure in a macroscopic model of a solidification process, *Metall. Trans. A* (1989), submitted.
32. A. Celmins, Representation of two-phase flows by volume averaging, *Int. J. Multiphase Flow* **14,** 81–90 (1988).
33. M. C. Flemings, *Solidification Processing*. McGraw-Hill, New York (1974).
34. D. K. Gartling, Finite element analysis of convective heat transfer problems with change of phase, *Comput. Meth. Fluids* 257–284 (1980).
35. C. Prakash and V. R. Voller, On the numerical solution of continuum mixture model equations describing binary solid–liquid phase change, *Numer. Heat Transfer B* **15,** 171–189 (1989).

## APPENDIX. PHYSICAL DERIVATION OF EQUATION (13)

Consider the microscopic control volume shown in Fig. A1. Assuming, without loss of generality, that the control volume has unit dimensions, the solute concentration at time $t$ is given by equation (11) as

$$\rho C_{\text{mix}} = \rho f_l C_l + \rho_s \int_0^{g_s} C_s \, d\alpha$$

$$= \rho f_l C_l + I. \tag{A1}$$

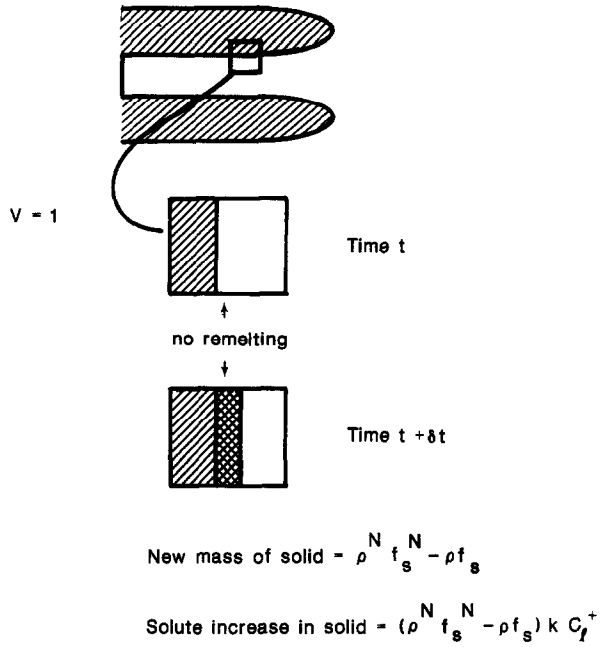


FIG. A1. Progression of solidification in microscopic volume element.

At time $t = t+\delta t$, under the assumption of no local remelting, the solute concentration is given by

$$\rho C_{mix} = \rho^n f_l^n C_l^n + I + [\rho^n f_s^n - \rho f_s] k C_l^+ \qquad (A2)$$

where $[\ ]^n$ indicates evaluation at time $t+\delta t$ and $C_l^+$ is interpreted as a representative value of $C_l$ over the time interval $[t, t+\delta t]$. (Note that as $\delta t \to 0$, $C_l^+ \to C_l$.) The last term on the right-hand side of equation (A2) represents the increase in the solute concentration in the solid due to the formation of new solid, over the time period $\delta t$. This is given by the product of the increase in the mass of solid formed (i.e. $[\rho^n f_s^n - \rho f_s]$), and the representative value of the solid concentration on the solid–liquid interface during that time interval. Equation (13) follows directly from equations (A1) and (A2) on utilizing the fundamental definition of a partial derivative, i.e.

$$\frac{\partial(\rho C_{mix})}{\partial t} = \lim_{\delta t \to 0} \frac{[\text{equation (A2)} - \text{equation (A1)}]}{\delta t}.$$

## MODELISATION DU TRANSFERT DE CHALEUR DE MASSE ET DE SOLUTE DANS LES SYSTEMES DE SOLIDIFICATION

**Résumé**—L'objet de ce texte est d'explorer le domaine du possible des modèles monophasiques de la solidification d'un alliage binaire. En partant d'une description générale diphasique, basée sur le modèle à deux fluides, trois cas limitatifs sont identifiés qui résultent en des modèles monophasiques de systèmes binaires. Chacun de ces modèles peut être facilement traduit en codes numériques pour écoulement de phase unique. On examine les différences entre les prédictions de ces modèles. On évalue, en particulier, les effets des modèles sur les configurations prédites de macro-ségrégation.

## MODELLIERUNG VON WÄRME-, MASSEN- UND LÖSUNGSTRANSPORT BEI DER VERFESTIGUNG

**Zusammenfassung**—Das Ziel dieser Abhandlung ist, den Anwendungsbereich von Einphasenmodellen bei der Verfestigung von binären Legierungen zu ermitteln. Ausgehend von einer allgemeinen Beschreibung der zweiphasigen Vorgänge aufgrund eines Zweiflüssigkeitenmodells werden drei Grenzfälle umrissen, die sich mit einphasiger Betrachtung abhandeln lassen. Jedes dieser Modelle kann leicht in Standardrechenprogrammen für Einphasenströmung implementiert werden. Unterschiede zwischen den Rechenergebnissen nach den einzelnen Modellen werden verglichen. Insbesondere werden die Einflüsse dieser Modelle auf die berechneten makroskopischen Entmischungsformen ermittelt.

## МОДЕЛИРОВАНИЕ ПЕРЕНОСА ТЕПЛА, МАССЫ И РАСТВОРЕННОГО ВЕЩЕСТВА ПРИ ЗАТВЕРДЕВАНИИ

**Аннотация**—Проведено исследование диапазона возможных однофазных моделей затвердевания бинарного сплава. С использованием общего описания двухфазного процесса на основе модели двух сред установлено существование трех предельных случаев, позволяющих получить однофазные модели бинарных систем. Каждая из моделей может быть легко реализована с помощью стандартных численных алгоритмов для однофазного течения. Рассматриваются различия между расчетами по предложенным моделям. В частности, оценивается влияние моделей на характеристики макроразделения.